Nodal Domain Statistics of Quantum Billiards

Rhine Samajdar [1] and Sudhir R. Jain [2]

[1]Indian Institute of Science, Bangalore 560012, India.

[2]Bhabha Atomic Research Centre, Mumbai 400085, India.

March 18, 2015.

Quantum chaos: Fundamentals and Applications Session Workshop I,

École des sciences avances de Luchon.

Table of Contents

1. Introduction
   - About Quantum Billiards
   - Motivation
   - General Mathematical Formulation
2. Separable Billiard Geometries
   - Cartesian coordinates
   - Polar and Elliptic coordinates
   - Parabolic coordinates
3. Non-separable Billiards
   - Right-angled isosceles triangle
   - $30^\circ - 60^\circ - 90^\circ$ hemiequilateral triangle
   - Equilateral triangle
4. Nodal Domain Statistics
5. Conclusion
6. References

Section Outline

1. Introduction
   - About Quantum Billiards
   - Motivation
   - General Mathematical Formulation
2. Separable Billiard Geometries
   - Cartesian coordinates
   - Polar and Elliptic coordinates
   - Parabolic coordinates
3. Non-separable Billiards
   - Right-angled isosceles triangle
   - $30^\circ - 60^\circ - 90^\circ$ hemiequilateral triangle
   - Equilateral triangle
4. Nodal Domain Statistics
5. Conclusion
6. References

About Quantum Billiards

A point particle moves freely inside an enclosure, reflecting specularly from the boundaries in accordance with Snells law.

The problem reduces to solving the Schrödinger equation for the system with Dirichlet boundary conditions.

Notation

$\mathcal{D} \subset \mathbb{R}^2$, a connected domain on a 2-dimensional Riemannian manifold,

$-\nabla^2 \Psi_j(\mathbf{r}) = E_j\, \Psi_j(\mathbf{r})$, $\mathbf{r} \in \mathcal{D}$ and $\Psi_j|_{\partial\mathcal{D}} = 0$.

A Criterion for Quantum Chaos

Nodal domains of a real wavefunction are the maximally connected regions wherein the function does not change sign.

- The distribution of the numbers of nodal domains ($\nu_{m,n}$) of Ψ in two dimensions distinguishes between systems with integrable (separable) or chaotic underlying classical dynamics.
  G. Blum, S. Gnutzmann and U. Smilansky, *Phys. Rev. Lett.* **88**, 114101 (2002).
- Let $\xi = \nu_j / j$ and $I_g(E) = [E, E + gE]$ ($g > 0$, arbitrary). Then,

$$P(\xi) = \lim_{E \to \infty} \frac{1}{N_I} \sum_{E_j \in I_g(E)} \delta\left(\xi - \frac{\nu_j}{j}\right).$$

Definitions

- Let $R_{k,n}$ be an equivalence relation defined on the set of wavefunctions as

$$R_{k,n} = \{(\Psi(m_1, n), \Psi(m_2, n)) : m_1 \equiv m_2 (\text{mod } kn)\}.$$

- The relation $R_{k,n}$ defines a partition $\mathcal{P}$ of the set of wavefunctions into equivalence classes $[\mathcal{C}_{kn}]$ where $\mathcal{C}_{kn} = m$ mod $k\,n$.

- Forward difference operator: $\Delta_t \mathcal{F}(x_1, x_2) = \mathcal{F}(x_1 + t, x_2) - \mathcal{F}(x_1, x_2)$.

The Nodal Domain Theorem

Nodal Domain Theorem for Integrable Billiards

If the metric space $\mathcal{D} \subset \mathbb{R}^2$ is integrable, then, in the absence of tiling, one of $\Delta_{kn}\nu\,(m,n) = \Phi(n)$ and $\Delta^2_{kn}\nu\,(m,n) = \Phi(n)$ holds $\forall\, m,n$ for some $\Phi : \mathbb{R} \to \mathbb{R}$, which is determined only by the geometry of the billiard.

Proof

This is demonstrated by verifying it individually for all possible integrable billiards on $\mathbb{R}^2$. The corresponding functions $\Phi(n)$ are calculated.

Only 6 geometries to be considered:

- Billiards separable in the coordinate systems:
  — Cartesian
  — Elliptic (including Polar)
  — Parabolic
- Non-separable billiards:
  — Right-angled isosceles triangle
  — $(30, 60, 90)$ hemiequilateral triangle
  — Equilateral triangle

Section Outline

1. Introduction
   - About Quantum Billiards
   - Motivation
   - General Mathematical Formulation
2. Separable Billiard Geometries
   - Cartesian coordinates
   - Polar and Elliptic coordinates
   - Parabolic coordinates
3. Non-separable Billiards
   - Right-angled isosceles triangle
   - $30^\circ - 60^\circ - 90^\circ$ hemiequilateral triangle
   - Equilateral triangle
4. Nodal Domain Statistics
5. Conclusion
6. References

The rectangle

$$\mathcal{D} = \left[0, L_x\right] \times \left[0, L_y\right] ; \alpha = L_x / L_y .$$

$$\Psi_{m,n} = \sqrt{\frac{4}{L_x L_y}} \sin\left(\frac{m\pi x}{L_x}\right) \sin\left(\frac{n\pi y}{L_y}\right).$$

Energy Spectrum: $E = m^2 + \alpha^2 n^2$.

Computing $\Phi(n)$

$$\Delta_n \nu\left(m,n\right) = \nu_{m+n,n} - \nu_{m,n} = n^2 .$$

Hence, $\nu_{m,n} = mn + C_r ;\; C_r = 0$.

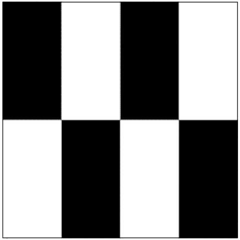

Figure: 'Checkerboard' pattern of nodal domains formed by an intersecting set of nodal lines for the quantum numbers $m = 4$ and $n = 2$.

The circle

$$\mathcal{D} = \{(x, y) : x^2 + y^2 \leq R^2\}.$$

$$\Psi_{m,n} = \frac{J_m(kr)}{\sqrt{\int_0^R [J_m(kr)]^2 r\,\mathrm{d}r}} \cdot \frac{\cos m\theta}{\sqrt{\pi}}; k = \sqrt{\frac{2\mu E}{\hbar^2}},$$

Energy Spectrum: $E = [z_{m,n}]^2$.

Computing $\Phi(n)$

$$\Delta_n \nu(m, n) = 2n^2 \qquad \text{if } m \neq 0.$$

Hence, $\nu_{m,n} = 2mn + C_c;\ C_c = 0.$

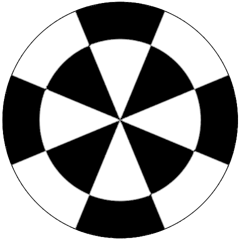

Figure: Nodal pattern of the circular billiard for the quantum numbers $m = 4$ and $n = 2$.

Generalisation to the ellipse

- Separable in elliptic coordinates, ξ and η.
- Ψ described in terms of the radial and angular Mathieu functions.

Computing $\Phi(n)$

$\Delta_\ell\, \nu\,(r,\ell) = \nu_{r+\ell,\,\ell} - \nu_{r,\,\ell} = 4\ell^2.$

Hence, $\nu_{r,\ell} = \ell(4r+2)+1$.

When $\ell = 0$, $\nu_{r,\,\ell} = r+1$,

thus, trivially, $\Delta_\ell\, \nu\,(r,\,0) = 4\ell^2 = 0$.

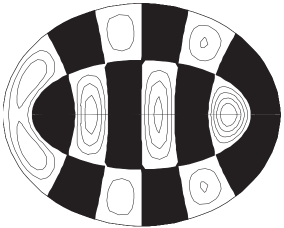

Figure: The elliptic billiard (of eccentricity $\sqrt{2}$) displays a similar pattern of nodal domains as observed in the $+\,-$ parity mode, symmetric about the X-axis.

Confocal parabolas and general arguments

Consider billiard motion in a domain bounded by confocal parabolas such that Ψ is separable in the parabolic coordinates σ and τ defined by

$$x = \sigma\tau \qquad \text{and} \qquad y = \frac{1}{2}\left(\tau^2 - \sigma^2\right).$$

- It is easy to see that the theorem holds with $\Delta_n \nu\,(m, n) \sim n^2$ since separability implies that $\nu_{m,n} = m\,n + \mathrm{O}\big(1\big)$, where m, n are the integer quantum numbers.

  G. Blum, S. Gnutzmann and U. Smilansky, *Phys. Rev. Lett.* **88**, 114101 (2002).

Observation

The same argument may be extended for all separable billiards, including annular regions and sectors of separable billiards.

Section Outline

1. Introduction
   - About Quantum Billiards
   - Motivation
   - General Mathematical Formulation
2. Separable Billiard Geometries
   - Cartesian coordinates
   - Polar and Elliptic coordinates
   - Parabolic coordinates
3. Non-separable Billiards
   - Right-angled isosceles triangle
   - $30^\circ - 60^\circ - 90^\circ$ hemiequilateral triangle
   - Equilateral triangle
4. Nodal Domain Statistics
5. Conclusion
6. References

Right-angled isosceles triangle

$$\mathcal{D} = \left\{(x,y) \in [0,\pi]^2 : y \leq x\right\} \qquad \psi_{m,n} = \sin(mx)\,\sin(ny) - \sin(nx)\,\sin(my).$$

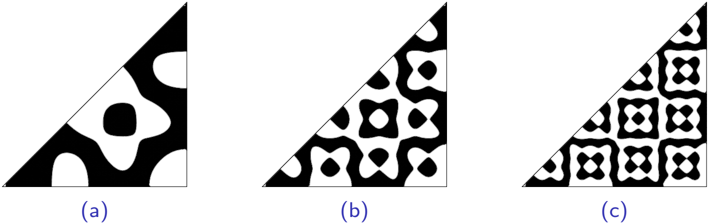

Figure: The pattern of nodal domains for (a) $\Psi_{7,4}$, (b) $\Psi_{15,4}$ and (c) $\Psi_{23,4}$. All the three eigenfunctions belong to the same equivalence class $[\mathcal{C}_{2n}]$ and the nodal patterns are similar as the wavefunction evolves from one state to another within members of the same class.

Domains are counted using the Hoshen-Kopelman algorithm.

J. Hoshen, R. Kopelman, *Phys. Rev. B.* **45**, 3438 (1976).

Nodal counts

m	n	$\mathcal{C}_{2n} = m \mod 2n$	$\nu_{m,n}$	$\Delta_{2n}\,\nu\,(m,n)$	$I_{m,n}$	$\Delta_{2n}\,I\,(m,n)$
38	13	12	103	–	78	–
64	13	12	194	91	156	78
90	13	12	285	91	234	78
116	13	12	376	91	312	78
142	13	12	467	91	390	78

Table: An illustration of the constancy of the first difference of $\nu_{m,n}$ and the nodal loop count, $I_{m,n}$, for the wavefunctions belonging to the same class.

An expression for $\nu_{m,n}$

- $\nu_{m+2n,n} - \nu_{m,n} = \frac{n^2+n}{2}$ so, $\nu_{m,n} = \frac{1}{4}m(n+1) + \alpha(n, \mathcal{C}_{2n})$.
- Let $\zeta_1 = n \mod \mathcal{C}_{2n}$ and $\zeta_2 = n \mod 2\mathcal{C}_{2n}$. When $\mathcal{C}_{2n}$ is even,

$$\nu_{m,n} = \frac{m(n+1)+n-2}{4} + \left[-\frac{n^2}{4} + \left(\frac{\mathcal{C}_{2n}}{2} \right) n - \left\{ \frac{\mathcal{C}_{2n}^2 - \mathcal{C}_{2n} - 1}{2} \pm \frac{1}{4}(\zeta_2 - 1) \right\} \right],$$

with the $+$ sign being applicable when $\mathcal{C}_{2n} < \zeta_2$ and the $-$ sign otherwise.

- When $\mathcal{C}_{2n}$ is odd,

$$\nu_{m,n} = \frac{m(n+1)+n-2}{4} + \left[-\frac{n^2}{4} + \left(\frac{\mathcal{C}_{2n}}{2} \right) n - \left\{ \frac{2\mathcal{C}_{2n}^2 - \mathcal{C}_{2n} - 2}{4} + \gamma \right\} \right].$$

- For $\zeta_1 = 1$, $\gamma = 0$ and for $\zeta_1 = \mathcal{C}_{2n} - 1$, γ exactly reduces to $\frac{1}{2}(\mathcal{C}_{2n} - 1)$. $\lim_{k\to\infty} \frac{\gamma}{\nu_{m+kn,n}} = 0$; γ is a term responsible for small fluctuations.

$30^\circ - 60^\circ - 90^\circ$ hemiequilateral triangle

The (30, 60, 90) scalene triangle correspond to the states of the equilateral triangle which are antisymmetric about the altitude.

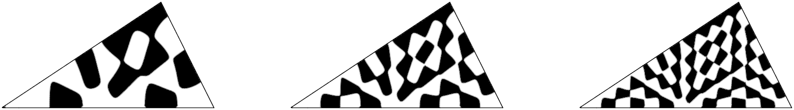

(a) (b) (c)

Figure: The nodal domains of the (30, 60, 90) triangle for (a) $\Psi_{11,2}$, (b) $\Psi_{17,2}$ and (c) $\Psi_{23,2}$.

$$\Delta^2_{3n}\,\nu\,(m,n) = \nu_{m+6n,n} - 2\nu_{m+3n,n} + \nu_{m,n} = 0.$$

Extensive analysis of a considerable number of lower states shows that, for the non-tiling situations, $\Delta_{3n}\,\nu(m,n) \approx n^2 + 1$.

Nodal counts

m	n	$\mathcal{C}_{3n}$	$\nu_{m,n}$	$\Delta_{3n}\,\nu\,(m,n)$	m	n	$\mathcal{C}_{3n}$	$\nu_{m,n}$	$\Delta_{3n}\,\nu\,(m,n)$
5	2	5	2	–	7	3	7	3	–
11	2	5	7	5	16	3	7	13	10
17	2	5	12	5	25	3	7	23	10
23	2	5	17	5	34	3	7	33	10
29	2	5	22	5	43	3	7	43	10

Table: Illustrative sample of data of the first difference of $\nu_{m,n}$ for the wavefunctions of the (30, 60, 90) triangle belonging to the same equivalence class.

Equilateral triangle

$$\mathcal{D} = \left\{(x,y) \in \left[0, \frac{\pi}{2}\right] \times \left[0, \frac{\sqrt{3}\pi}{2}\right] : y \leq \sqrt{3}x\right\} \cup \left\{(x,y) \in \left[\frac{\pi}{2}, \pi\right] \times \left[0, \frac{\sqrt{3}\pi}{2}\right] : y \leq \sqrt{3}(\pi - x)\right\}.$$

$$\begin{aligned}\Psi^{c,s}_{m,n}(x,y) \quad &= \quad (\cos,\sin)\left[(2m-n)\frac{2\pi}{3L}x\right]\sin\left(n\frac{2\pi}{\sqrt{3}L}y\right) - (\cos,\sin)\left[(2n-m)\frac{2\pi}{3L}x\right]\sin\left(m\frac{2\pi}{\sqrt{3}L}y\right) \\ &+ \quad (\cos,\sin)\left[-(m+n)\frac{2\pi}{3L}x\right]\sin\left[(m-n)\frac{2\pi}{\sqrt{3}L}y\right].\end{aligned}$$

(a) (b) (c)

Figure: The evolution of the pattern of nodal domains of the equilateral triangle from (a) $\Psi_{16,5}$ to (b) $\Psi_{31,5}$ and finally, to (c) $\Psi_{46,5}$.

Nodal counts

m	n	$\mathcal{C}_{3n}$	$\nu_{m,n}$	$\Delta_{3n}\nu(m,n)$	$I_{m,n}$	$\Delta_{3n}I(m,n)$	$\Delta^2_{3n}\nu(m,n) = \Delta^2_{3n}I(m,n)$
24	7	3	44	–	21	–	–
45	7	3	198	154	154	133	–
66	7	3	499	301	434	280	147
87	7	3	947	448	861	427	147
108	7	3	1542	595	1435	574	147

Table: An example showing the values of the second difference of $\nu_{m,n}$ for the wavefunctions on the equilateral triangle corresponding to the same class, defined by $m \mod 3n$.

An expression for $\nu_{m,n}$

- $\nu_{m+6n,n} - 2\nu_{m+3n,n} + \nu_{m,n} = 3n^2.$
- $\nu_{m,n} = \frac{3}{2}\left(\frac{m^2}{9} - \frac{mn}{3}\right) + \frac{m\ \alpha(n,\mathcal{C}_{3n})}{3n} + \beta(n,\mathcal{C}_{3n})$
- $$\begin{aligned} \nu_{m,n} &= \frac{m^2}{6} - \frac{(4n-3)m}{6} + n^2 - \frac{\mathcal{C}_{3n}n - \lambda_1(\mathcal{C}_{3n},n)}{3} && \text{if } 0 < \mathcal{C}_{3n} < n, \\ &= \frac{m^2}{6} - \frac{(4n-3)m}{6} + n^2 - \frac{2(\mathcal{C}_{3n}-n)n - \lambda_2(\mathcal{C}_{3n},n)}{3} && \text{if } n < \mathcal{C}_{3n} < 3n. \end{aligned}$$

λ_1 and λ_2 contribute to small variations in the nodal domain count.

- $\lambda_1(\mathcal{C}_{3n},\mathcal{C}_{3n}+1) = \mathcal{C}_{3n}^2 + 3,$
  $\lambda_2(\mathcal{C}_{3n},2\mathcal{C}_{3n}+1) = \lambda_2(\mathcal{C}_{3n},2\mathcal{C}_{3n}+2) = \mathcal{C}_{3n}(\mathcal{C}_{3n}+3).$

Section Outline

1. Introduction
   - About Quantum Billiards
   - Motivation
   - General Mathematical Formulation
2. Separable Billiard Geometries
   - Cartesian coordinates
   - Polar and Elliptic coordinates
   - Parabolic coordinates
3. Non-separable Billiards
   - Right-angled isosceles triangle
   - $30^\circ - 60^\circ - 90^\circ$ hemiequilateral triangle
   - Equilateral triangle
4. Nodal Domain Statistics
5. Conclusion
6. References

The distribution function of ξ

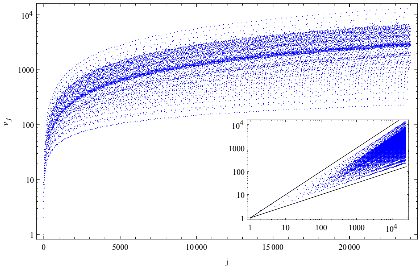

Figure: The number of nodal domains for the equilateral triangle billiards for the first 12045 wavefunctions (in increasing order of energy).

Inset: The corresponding plot of log ν_j against log j. The figure, bounded by straight lines of slopes 0.5 and 1, shows the scaling of ν_j with j as $j \to \infty$.

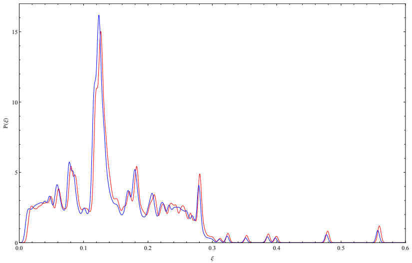

Figure: $P[\xi, I_\lambda(E)]$ for the equilateral triangle billiard in the spectral intervals $[10000, 20000]$ (red) and $[20000, 40000]$ (blue).

Pleijel's bound:

$$\overline{\lim_{j\to\infty}} \frac{\nu_j}{j} \leq \left(\frac{2}{j_0}\right)^2 \approx 0.691.$$

The cumulative nodal loop count

$$C(N) := \sum_{j=1}^{\lfloor N \rfloor} I_j$$

$$V(k) := \sum_{j=1}^{\infty} I_j \Theta(k - k_j)$$

A. Aronovitch et al., *J. Phys. A: Math. Theor.* **45**, 085209 (2012).

Periodic orbits

$$L_{p,q} = a\sqrt{3(p^2 + pq + q^2)},$$

where $(p, q) \in \mathbb{Z}^2 \backslash (0, 0)$. The initial angle, with respect to the horizontal, is:

$$\tan^{-1}\left(\frac{p - q}{(p + q)\sqrt{3}}\right)$$

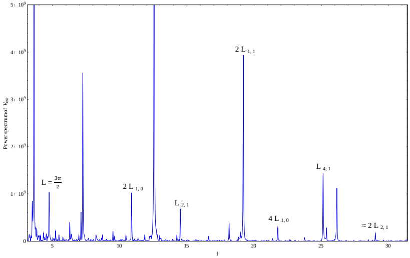

Figure: The power spectrum obtained on Fourier transforming the oscillatory part of the cumulative counting function, $V(k)$.

The cumulative nodal loop count

$$C(N) := \sum_{j=1}^{\lfloor N \rfloor} I_j$$

$$V(k) := \sum_{j=1}^{\infty} I_j \Theta(k - k_j)$$

A. Aronovitch et al., *J. Phys. A: Math. Theor.* **45**, 085209 (2012).

Periodic orbits

$$L_{p,q} = a\sqrt{3(p^2 + pq + q^2)},$$

where $(p, q) \in \mathbb{Z}^2 \backslash (0, 0)$. The initial angle, with respect to the horizontal, is:

$$\tan^{-1}\left(\frac{p - q}{(p + q)\sqrt{3}}\right)$$

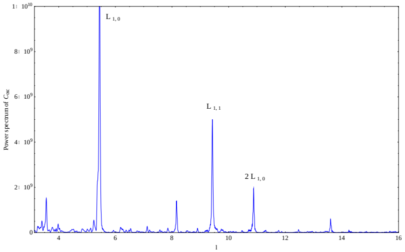

Figure: The power spectrum obtained on Fourier transforming the oscillatory part of $C(N)$ with respect to the scaled variable c.

Section Outline

1. Introduction
   - About Quantum Billiards
   - Motivation
   - General Mathematical Formulation
2. Separable Billiard Geometries
   - Cartesian coordinates
   - Polar and Elliptic coordinates
   - Parabolic coordinates
3. Non-separable Billiards
   - Right-angled isosceles triangle
   - $30^\circ - 60^\circ - 90^\circ$ hemiequilateral triangle
   - Equilateral triangle
4. Nodal Domain Statistics
5. Conclusion
6. References

Conclusions

- In this presentation, for *all* integrable systems, we see that the number of domains, $\nu_{m,n}$ of an eigenfunction satisfies a difference equation.
- As classifying patterns in non-separable shapes and counting domains has been a very difficult problem, the theorem presented here marks a considerable advance.
- In short, *the geometrical patterns have been algebraically represented*.

References

- R.S. and S. R. Jain, A nodal domain theorem for integrable billiards in two dimensions, *Ann. Phys.* **351**, 1–12 (2014).
- R.S. and S. R. Jain, Nodal domains of the equilateral triangle billiard, *J. Phys. A: Math. Theor.* **47**, 195101 (2014).

Thank you!